Available online at www.sciencedirect.com
ScienceDirect
Journal of Power Sources 174 (2007) 673–677
JOURNAL OF POWER SOURCES
www.elsevier.com/locate/jpowsour

Short communication

Thermal properties of $Li_{4/3}Ti_{5/3}O_4$/$LiMn_2O_4$ cell

W. Lu *, I. Belharouak, J. Liu, K. Amine

Chemical Engineering Division, Argonne National Laboratory, 9700 S. Cass Avenue, Argonne, IL 60439, United States

Available online 30 June 2007

Abstract

The thermal properties of $Li_{4/3}Ti_{5/3}O_4$ and $Li_{1+x}Mn_2O_4$ electrodes were investigated by isothermal micro-calorimetry (IMC). The 150-mAh g^{-1} capacity of a Li/$Li_{4/3}Ti_{5/3}O_4$ half cell was obtained through the voltage plateau that occurs at 1.55 V during the phase transition from spinel to rock salt. Extra capacity below 1.0 V was attributed to the generation of a new phase. The small and constant entropy change of $Li_{4/3}Ti_{5/3}O_4$ during the spinel/rock-salt phase transition indicated its good thermal stability. Accelerated rate calorimetry confirmed that $Li_{4/3}Ti_{5/3}O_4$ has better thermal characteristics than graphite. The IMC results for a Li/$Li_{1+x}Mn_2O_4$ half cell indicated less heat variation due to the suppression of the order/disorder change by lithium doping. The heat profiles of the $Li_{4/3}Ti_{5/3}O_4$/$Li_{1+x}Mn_2O_4$ full cell indicated less heat generation compared with a mesocarbon-microbead graphite/$Li_{1+x}Mn_2O_4$ cell.
Published by Elsevier B.V.

Keywords: Lithium titanate spinel; Lithium manganese spinel; Entropy change; Thermal safety

1. Introduction

Recently, safety has become a major concern for lithium ion batteries. It is well known that both carbon anodes and layered metal oxide cathodes have safety issues because of their intrinsic thermal properties in the fully charged state. For instance, fully charged lithium metal oxide can release oxygen, which oxidizes the solvent and generates enough heat to cause a cell thermal runaway. To improve the thermal characteristics of lithium ion batteries, electrode materials that are more thermally stable should be developed to replace the current materials.

$Li_{1+x}Mn_{2-x}O_4$ ($x=0.156$) spinel is a promising candidate for the cathode due to its excellent safety, low cost, good power capability, and low toxicity. Moreover, because of lithium doping, the capacity retention of a $Li_{1+x}Mn_{2-x}O_4$ spinel based cell is improved [1,2] compared with stoichiometric $LiMn_2O_4$. Furthermore, the residual lithium ion remaining in the structure may stabilize the material and prevent oxygen loss at the end of charge.

As for the anode, $Li_{4/3}Ti_{5/3}O_4$ ($Li_{8a}[Li_{1/3}Ti_{5/3}]_{16d}O_4$) has been proposed as a promising candidate [3]. This material can accommodate lithium ions during the charging process, resulting in a structural transition from $Li_{8a}[Li_{1/3}Ti_{5/3}]_{16d}O_4$ spinel to $[Li_2]_{16c}[Li_{1/3}Ti_{5/3}]_{16d}O_4$ rock-salt phase without a noticeable change in lattice parameter. Intensive studies have demonstrated that this so-called "zero-strain material" offers excellent cycle life without capacity fade after hundreds of cycles [4–7]. Moreover, $Li_{4/3}Ti_{5/3}O_4$ may not form a solid electrolyte interface (SEI) and can operate well with propylene carbonate solvent without the risk of exfoliation [8]. These features could make a cell based on $Li_{4/3}Ti_{5/3}O_4$ spinel operate safely at both low and high temperatures.

In this study, we determined the electrochemical behavior and thermal properties of Li/$Li_{4/3}Ti_{5/3}O_4$ and Li/$Li_{1+x}Mn_2O_4$ spinel by isothermal micro-calorimetry (IMC). In addition, the heat generation of a $Li_{4/3}Ti_{5/3}O_4$/$Li_{1+x}Mn_2O_4$ full cell was determined and compared with a cell using a $Li_{1+x}Mn_2O_4$ cathode and mesocarbon-microbead (MCMB) graphite anode.

2. Experimental

$Li_{4/3}Ti_{5/3}O_4$ spinel was synthesized by a solid-state reaction with anatase TiO_2 and Li_2CO_3 at 800 °C. The $Li_{4/3}Ti_{5/3}O_4$ electrode consists of a mixture of 80% by weight of active material, 10% poly-vinylidene difluoride (PVDF) binder, and 10% carbon black. Li/$Li_{4/3}Ti_{5/3}O_4$ half cells were fabricated in a glove box. These cells had a counter electrode (lithium metal), porous separator (Celgard 3501), and an electrolyte consisting of a 3:7 wt% mixture of ethylene carbonate (EC) and diethyl carbon-

* Corresponding author. Current address: Greatbatch, Inc., 10000 Wehrle Dr., Clarence, NY 14031, United States. Tel.: +1 716 759 5349; fax: +1 716 759 5480.
E-mail address: wlu@greatbatch.com (W. Lu).

0378-7753/$ – see front matter. Published by Elsevier B.V.
doi:10.1016/j.jpowsour.2007.06.199

ate (EMC) solvent with 1.2 M $LiPF_6$ salt. The total capacity of 2.0 mAh can be obtained when this button cell is cycled between 1.8 and 0.2 V.

An isothermal micro-calorimeter (model CSC 4400, Calorimetry Science Corp.) was used to measure the heat rate of the cells while the temperature was kept at 25 °C throughout the experiment. (The details of IMC operation and analysis can be found in Refs. [9–11].) The total heat rate obtained by IMC consists of the irreversible heat rate (q_{irr}) and the reversible heat rate (q_{rev}). The charged $Li_{4/3}Ti_{5/3}O_4$ and graphite were also tested by accelerated rate calorimetry (ARC).

The $Li_{1.156}Mn_{1.844}O_4$ used in this study was received from Toda (Japan). The positive laminates in this study consisted of 82% active material, 10% carbon additive (TB5500), and 8% PVDF. The following cells with the electrolyte and separator described above were prepared for the IMC test: $Li/Li_{1.156}Mn_{1.844}O_4$, $Li/Li_{4/3}Ti_{5/3}O_4$, $MCMB/Li_{1.156}Mn_{1.844}O_4$, and $Li_{4/3}Ti_{5/3}O_4/Li_{1.156}Mn_{1.844}O_4$. The capacity of all the cells is 1.1 mAh limited by $Li_{1.156}Mn_{1.844}O_4$ with 9/16 in. diameter.

The cut-off voltages were between 2.7 and 1.7 V for $Li_{4/3}Ti_{5/3}O_4/Li_{1.156}Mn_{1.844}O_4$ and between 4.2 and 3.0 V for $MCMB/Li_{1.156}Mn_{1.844}O_4$ cells. Both cells were subjected to different charge rates based on the capacity of the cathode material.

3. Results and discussion

Fig. 1 shows the voltage and heat flow profiles of the $Li/Li_{4/3}Ti_{5/3}O_4$ half cell during charge and discharge. A voltage plateau appears around 1.55 V with 150 mAh g^{-1} capacity followed by a sharp voltage drop. This voltage plateau is related to a transition from the spinel to the rock-salt phase. The constant heat flow along the voltage plateau (at 1.55 V) corresponds to the spinel/rock-salt transition. At the end of the two-phase transition, further lithium insertion leads to a series of heat variations, which are correlated to a series of voltage variations below 1.0 V. These variations in the voltage and heat flow profiles might be related to a order/disorder transition and the formation of a new phase [6,12]. During discharge, the reverse voltage and heat flow profiles are observed.

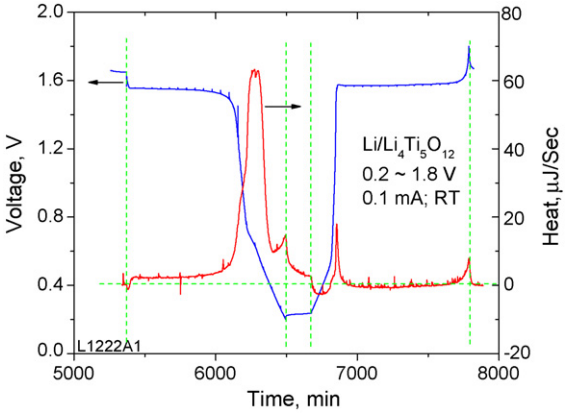

Fig. 1. Voltage and heat flow profiles of $Li/Li_{4/3}Ti_{5/3}O_4$ half cell during charge and discharge at room temperature (RT).

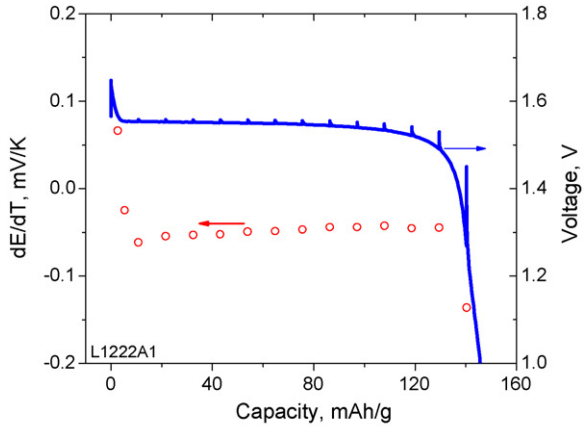

Fig. 2. Voltage profile and dE/dT results of $Li/Li_{4/3}Ti_{5/3}O_4$ half cell.

The irreversible heat of the cell can be calculated from the over-potential results. The reversible heat can be then calculated by subtracting the irreversible heat from the IMC results, based on the energy balance equation:

$$q = i(E_{ocv} - E) - iT(\partial E/\partial T)_P$$

In this equation, q stands for the heat flow rate of the cell, which is positive when the cell generates heat. The current, i, is positive for the cathodic reaction. The cell temperature, T (K), and pressure in the half cell, P, are considered constant during the IMC experiment. In addition, E_{ocv} stands for open-circuit voltage, E stands for the cell voltage during cycling, and dE/dT can be calculated by dividing the reversible heat with the term iT.

The calculated dE/dT results in the voltage plateau region between 1.8 and 1.0 V are shown in Fig. 2. The dE/dT curve as well as the voltage plateau is expected to be constant during the two-phase transition. The calculated dE/dT is around -0.05 mV K^{-1}, which is much smaller than that of graphite (-0.1 to 0.28 mV K^{-1}) [11]. The small entropy change is attributed to the zero change in the unit cell parameters of $Li_{4/3}Ti_{5/3}O_4$, which result in less heat generation by the cell related to the entropy change. The better thermal stability of $Li_{4/3}Ti_{5/3}O_4$ compared with graphite is confirmed by ARC, as shown in Fig. 3. The exothermic heat starts at about 200 °C. The corresponding temperature is much lower for graphite (100 °C) because of the SEI decomposition.

Fig. 4a shows the voltage and heat flow profiles of the $Li/Li_{1.156}Mn_{1.844}O_4$ cell during the charge and discharge. At the beginning of the charge, endothermic heat is observed, followed by a negligible and constant heat flow, until the cell reaches 4.1 V. In this case, no heat variation occurs around 3.9–4.0 V, as observed in the case of stoichiometric spinel [13,14]. This heat variation is attributed to an order–disorder change within the spinel framework. Such order–disorder change is suppressed when the spinel is doped with lithium. Therefore, doping the Mn spinel with lithium will lead not only to better thermal stability, but also to better cell performance with good structural integrity.

Fig. 4b shows the dE/dT results of $Li/Li_{1.156}Mn_{1.844}O_4$ cell using the same dE/dT calculation method for $Li/Li_{4/3}Ti_{5/3}O_4$

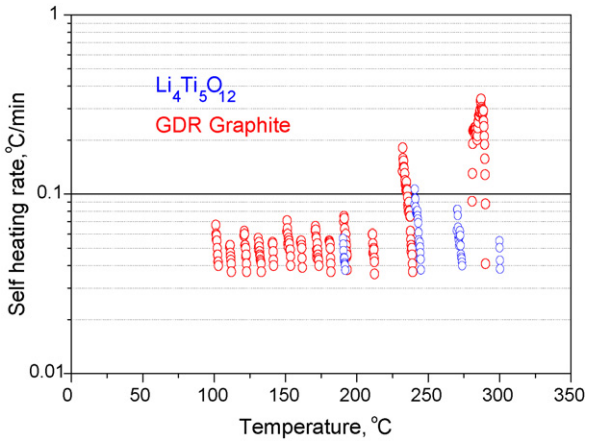

Fig. 3. ARC results of charged graphite and $Li_{4/3}Ti_{5/3}O_4$.

half cell. The dE/dT curve for $LiMn_2O_4$ shows the same trend as the heat flow profile during the charge, which reflects the major contribution of the reversible heat. The flat dE/dT in the middle of the SOC is due to the reduction of the phase transition of $Li_{1.156}Mn_{1.844}O_4$.

Fig. 5a and b show the heat flow profiles of the $Li_{4/3}Ti_{5/3}O_4$/$Li_{1.156}Mn_{1.844}O_4$ and MCMB/$Li_{1.156}Mn_{1.844}O_4$ cells during charge and discharge at the same current −0.1 mA (C/10). The heat profile of the $Li_{4/3}Ti_{5/3}O_4$/$Li_{1.156}Mn_{1.844}O_4$ cell has the same shape as that of the Li/$Li_{1.156}Mn_{1.844}O_4$ half cell, whereas the heat flow profile of the MCMB/$Li_{1.156}Mn_{1.844}O_4$ cell has the same shape as that of the Li/MCMB cell [11]. The reason for this behavior is that the heat flow of the cells at low cycling charge rate reflects the reversible heat effect, which is related to the dE/dT results. For the $Li_{4/3}Ti_{5/3}O_4$/$Li_{1.156}Mn_{1.844}O_4$ cell, the dE/dT of $Li_{4/3}Ti_{5/3}O_4$ is constant and small. Therefore, the reversible heat effect of $Li_{1.156}Mn_{1.844}O_4$ is more dominant. As for the MCMB/$Li_{1+x}Mn_{2-x}O_4$ cell, the reversible heat effect of MCMB is more dominant. Thus, the heat flow profile follows the shape of the Li/MCMB half cell. Fig. 5 also indicates that the heat flow curves during the charge and discharge are relatively symmetrical to each other except at the end of the charge and discharge. Again, this behavior can be attributed to the dominant effect of the reversible heat of the cells, since it makes an opposite contribution to the total heat due to the different sign of the current (see energy balance equation) during charge and discharge.

Fig. 6a and b show the heat profiles of $Li_{4/3}Ti_{5/3}O_4$/$Li_{1+x}Mn_2O_4$ and MCMB/$Li_{1+x}Mn_2O_4$ cells during charge at 0.1 mA (C/10) and 1.0 mA (1 C), respectively. For both charge rates, the heat variation of the MCMB/$Li_{1.156}Mn_{1.844}O_4$ cell is larger than that of the $Li_{4/3}Ti_{5/3}O_4$/$Li_{1.156}Mn_{1.844}O_4$ cell due to the higher dE/dT variation of the MCMB.

Fig. 7 shows the total heat generation of $Li_{4/3}Ti_{5/3}O_4$/$Li_{1.156}Mn_{1.844}O_4$ and MCMB/$Li_{1.156}Mn_{1.844}O_4$ cells during the

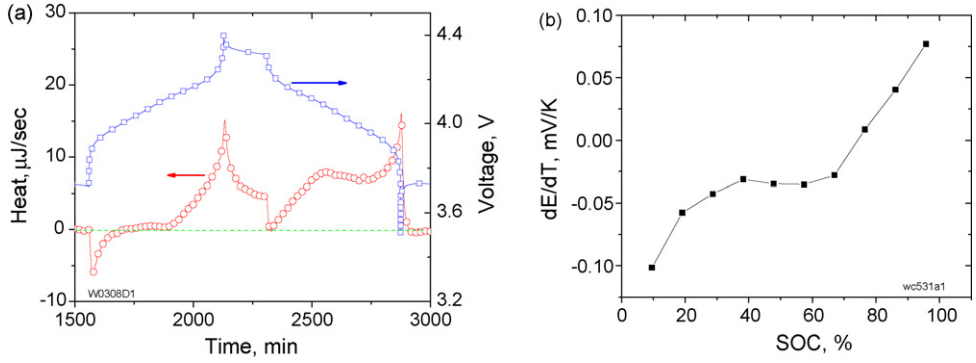

Fig. 4. (a) Voltage and heat flow profiles of Li/$Li_{1.156}Mn_{1.844}O_4$ cell during the charge and discharge and (b) dE/dT results vs. state of charge (SOC) for Li/$Li_{1+x}Mn_2O_4$ cell.

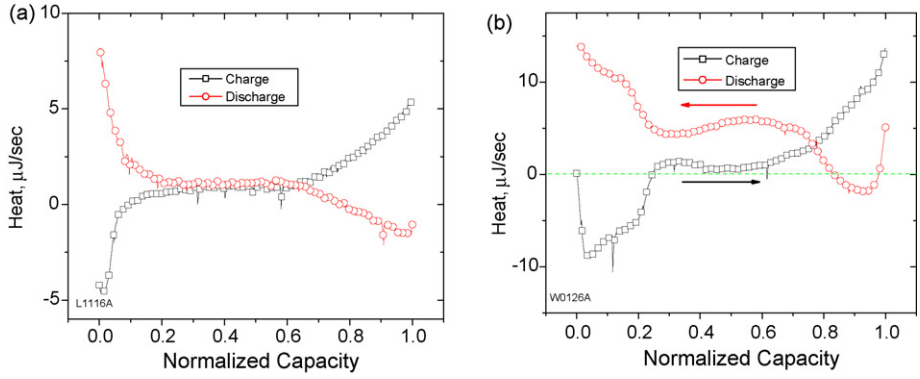

Fig. 5. Heat flow profiles of (a) $Li_{4/3}Ti_{5/3}O_4$/$Li_{1.156}Mn_{1.844}O_4$ and (b) MCMB/$Li_{1.156}Mn_{1.844}O_4$ cells as a function of normalized capacity.

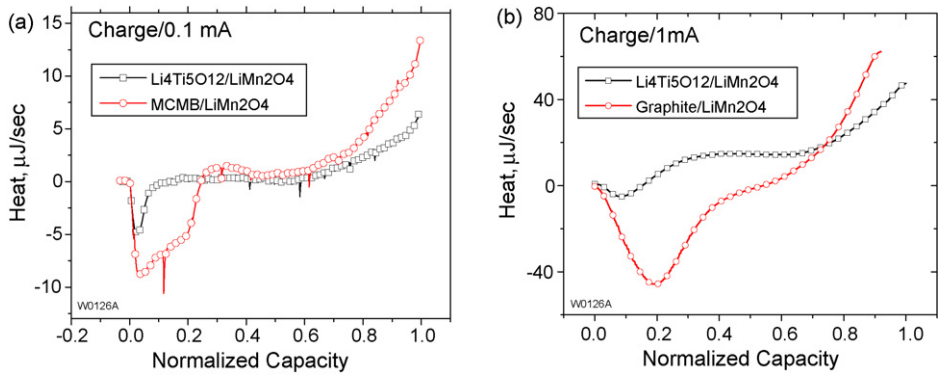

Fig. 6. Heat flow profiles of $Li_{4/3}Ti_{5/3}O_4/Li_{1.156}Mn_{1.844}O_4$ and MCMB/$Li_{1.156}Mn_{1.844}O_4$ cells as a function of normalized capacity at (a) 0.1 mA and (b) 1 mA charge rate.

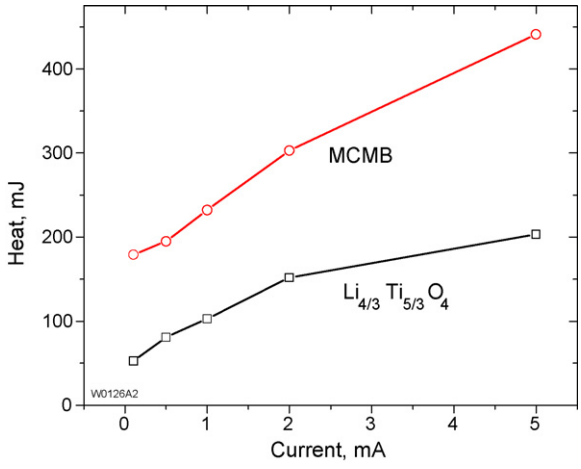

Fig. 7. Total heat generation of $Li_{4/3}Ti_{5/3}O_4/Li_{1.156}Mn_{1.844}O_4$ and MCMB/$Li_{1.156}Mn_{1.844}O_4$ cells during the charge processes as a function of the charge rate.

charge as a function of the charge rates. These curves were obtained by integrating the heat flow curves including the heat during the rest period, since the heat flow will not go to equilibrium immediately at the end of the charge and discharge due to the delay in the IMC response. It can be seen clearly that the total heat generation of the cell with the $Li_{4/3}Ti_{5/3}O_4$ anode is smaller than that with the MCMB anode. This result indicates that the $Li_{4/3}Ti_{5/3}O_4/Li_{1.156}Mn_{1.844}O_4$ cell has less heat generation and better thermal safety.

4. Conclusions

The heat generation of $Li/Li_{4/3}Ti_{5/3}O_4$ and $Li/Li_{1.156}Mn_{1.844}O_4$ half cells was investigated by IMC. The calculated dE/dT of $Li/Li_{4/3}Ti_{5/3}O_4$ is around $-0.05\,mV\,K^{-1}$ within a very narrow range $-0.04\,mV\,K^{-1}$. The ARC result indicates that the onset temperature of the exothermic reaction of the fully charged $Li_{4/3}Ti_{5/3}O_4$ is higher than that of fully charged MCMB graphite. Therefore, better thermal properties compared to graphite are expected for the $Li_{4/3}Ti_{5/3}O_4$ under different cycling conditions and charged states. Also, the IMC results of $Li/Li_{1.156}Mn_{1.844}O_4$ half cells show that the order–disorder change that occurred around 4.0–3.9 V in the case of stoichiometric $LiMn_2O_4$ is suppressed after the lithium doping, resulting in lower heat generation and less variation of dE/dT.

$Li_{4/3}Ti_{5/3}O_4/Li_{1.156}Mn_{1.844}O_4$ and MCMB/$Li_{1.156}Mn_{1.844}O_4$ cells were also investigated by IMC. The results show that the $Li_{4/3}Ti_{5/3}O_4/Li_{1.156}Mn_{1.844}O_4$ cell has less heat variation compared to the MCMB/$Li_{1.156}Mn_{1.844}O_4$ cell due to the constant and smaller entropy change of $Li_{4/3}Ti_{5/3}O_4$. Furthermore, the total heat generation of the $Li_{4/3}Ti_{5/3}O_4/Li_{1.156}Mn_{1.844}O_4$ cell is less compared to the MCMB/$Li_{1.156}Mn_{1.844}O_4$ cell at the different cycling rates. All these advanced thermal properties of $Li_{4/3}Ti_{5/3}O_4$/manganese spinel cell make this type of lithium ion batteries a possible system for higher power and longer cycle life applications, such as the lead-free accumulator as proposed by Ohzuku and Ariyoshi [15].

Acknowledgments

This work was performed under the auspices of the U.S. Department of Energy, Energy Efficiency and Renewable Energy, Office of FreedomCAR and Vehicle Technologies, under Contract No. W-31-109-Eng-38.

References

[1] K. Amine, H. Tukamoto, H. Yasuda, Y. Fujita, J. Electrochem. Soc. 143 (5) (1996) 1607–1613.
[2] R.J. Gummow, A. Dekock, M.M. Thackeray, Solid State Ionics 69 (1) (1994) 59–67.
[3] T. Ohzuku, A. Ueda, N. Yamamoto, J. Electrochem. Soc. 142 (5) (1995) 1431–1435.
[4] C.H. Chen, J.T. Vaughey, A.N. Jansen, D.W. Dees, A.J. Kahaian, T. Goacher, M.M. Thackeray, J. Electrochem. Soc. 148 (1) (2001) A102–A104.
[5] M. Venkateswarlu, C.H. Chen, J.S. Do, C.W. Lin, T.C. Chou, B.J. Hwang, J. Power Sources 146 (1/2) (2005) 204–208.
[6] A.D. Robertson, H. Tukamoto, J.T.S. Irvine, Electrochem. J. Soc. 146 (11) (1999) 3958–3962.
[7] A.N. Jansen, A.J. Kahaian, K.D. Kepler, P.A. Nelson, K. Amine, D.W. Dees, D.R. Vissers, M.M. Thackeray, J. Power Sources 81/82 (1999) 902–905.
[8] X.L. Yao, S. Xie, C.H. Chen, Q.S. Wang, J.H. Sun, Y.L. Li, S.X. Lu, Electrochim. Acta 50 (20) (2005) 4076–4081.

[9] W. Lu, H. Yang, J. Prakash, Electrochim. Acta 51 (7) (2005) 1322–1329.
[10] H. Yang, J. Prakash, J. Electrochem. Soc. 151 (2004) A1222.
[11] W. Lu, J. Prakash, J. Electrochem. Soc. 150 (2003) A262.
[12] W. Lu, I. Belharouak, J. Liu, K. Amine, J. Electrochem. Soc. 154 (2) (2007) A114–A118.
[13] H. Bang, H. Yang, Y.K. Sun, J. Prakash, J. Electrochem. Soc. 152 (2) (2005) A421–A428.
[14] J.-S. Kim, J. Prakash, J.R. Selman, Electrochem. Solid-State Lett. 4 (2001) A141.
[15] T. Ohzuku, K. Ariyoshi, Chem. Lett. 35 (8) (2006) 848.